

This document is confidential and is proprietary to the American Chemical Society and its authors. Do not copy or disclose without written permission. If you have received this item in error, notify the sender and delete all copies.

Understanding the Role of SEI Layer in Low Temperature Performance of Lithium-Ion Batteries

Journal:	<i>ACS Applied Materials & Interfaces</i>
Manuscript ID	am-2021-23934r.R1
Manuscript Type:	Article
Date Submitted by the Author:	n/a
Complete List of Authors:	Yoo, Dong-Joo; Argonne National Laboratory Liu, Qian; Argonne National Laboratory Cohen, Orion; UC Berkeley Kim, Minkyu; Argonne National Laboratory, Persson, Kristin; E O Lawrence Berkeley National Laboratory, Energy Technologies Area; UC Berkeley, Materials Science and Engineering Zhang, Zhengcheng; Argonne National Laboratory,

SCHOLARONE™
Manuscripts

1
2
3
4 **Understanding the Role of SEI Layer in Low Temperature Performance of**
5
6
7 **Lithium-Ion Batteries**
8
9

10 Dong-Joo Yoo,¹ Qian Liu,¹ Orion Cohen,² Minkyu Kim,¹ Kristin A. Persson,^{3,4} and
11 Zhengcheng Zhang^{1,*}
12
13

14
15
16 ¹Chemical Sciences and Engineering Division, Argonne National Laboratory, Lemont, IL
17 60439, USA
18
19

20
21 ²Department of Chemistry, University of California, Berkeley, Berkeley, CA 94720, USA
22
23

24 ³Department of Materials Science and Engineering, University of California, Berkeley,
25 Berkeley, CA 94720, USA
26
27

28
29 ⁴Molecular Foundry, Lawrence Berkeley National Laboratory, Berkeley, CA 94720, USA
30
31

32 *Corresponding author
33

34 E-mail: zzhang@anl.gov
35
36
37
38
39

40 **Keywords:** Solid-electrolyte-interface, graphite electrodes, butyronitrile-based electrolytes,
41 low temperature performance, lithium-ion batteries
42
43
44
45
46
47
48
49
50
51
52
53
54
55
56
57
58
59
60

Abstract

Low temperature electrolyte (LTE) has been considered as one of the most challenging aspects of wide adoption of lithium-ion batteries (LIB) since the SOA electrolytes cannot sufficiently support the redox reactions at LT resulting in dramatic performance degradation. Although many attempts have been taken by employing various non-carbonate solvents, there was a lack of fundamental understanding of the limiting factors for low temperatures operation (e.g. $-20^{\circ}\text{C} \sim -40^{\circ}\text{C}$). In this paper, we demonstrate the crucial role of the solid-electrolyte-interface (SEI) in LIB performance at low temperature using a butyronitrile (BN)-based electrolyte. Our results suggested that an additive formed SEI with low resistance and low charge transfer dictates the LT performance in terms of capacity and cycle life presenting a useful guideline in designing new electrolytes to address the LT issue.

Introduction

Since their commercialization, lithium-ion batteries (LIBs) have transformed our society, providing unprecedented freedom of mobility.¹⁻² LIBs have been a key device not only in portable electronics such as smart phones, smart watches, and laptops, but also in applications for environmentally harsh conditions such as drones, space exploration, and defense.³ While many aspects of LIB performance need to be improved, low temperature capability is the most challenging, since the conventional electrolytes cannot operate properly at sub-zero temperatures due to sharp drops in capacity and rate capability.⁴⁻⁵

At low temperature, LIBs have intrinsically slow kinetics at the interface, in the bulk electrolyte and in the active electrode materials. Li^+ has insufficient thermal energy for ion transfer at the interfaces or ion diffusion within the bulk electrolyte and active materials, so it cannot supply

1
2
3
4 the current density normally required during charge and discharge process at room
5
6 temperature.⁶⁻⁷ The sluggish kinetics at every level cause high cell impedance and contributes
7
8 to a large cell overpotential, resulting in lowered capacity and energy. In addition, during the
9
10 charging process, the large overpotential at the graphite anode causes lithium plating which not
11
12 only impairs the cell performance, but also exacerbates safety issues associated with a potential
13
14 short-circuit.⁸⁻⁹ Furthermore, since there are many factors affecting the performance at low
15
16 temperature such as the active materials, electrolytes, and electrode configurations, it is hard
17
18 to pinpoint the actual limiting factor and find a solution to address the issue.
19
20
21
22

23
24
25 Conventional LIB electrolytes are based on a mixture of carbonate solvents dissolved with a
26
27 lithium salt. The cyclic carbonate, ethylene carbonate (EC), is known to be an indispensable
28
29 component due to its unique capability of forming a stable solid-electrolyte-interphase (SEI).¹⁰⁻
30
31 ¹¹ This SEI passivates the graphite surface, preventing the continuous reaction of electrolyte
32
33 components with lithiated graphite, and enabling the reversible intercalation/deintercalation
34
35 chemistry of LIBs. However, EC has a high melting point of 34°C (solid state at room
36
37 temperature), therefore electrolytes with high portion of EC for example > 50 vol% have
38
39 adversely affected ionic conductivity at temperatures below -20°C.¹² Tertiary¹³⁻¹⁴ and
40
41 quaternary¹⁵⁻¹⁶ carbonate solvent systems with low portion of EC have been proposed and
42
43 studied for low temperature application.
44
45
46
47
48
49

50
51 Carbonate derivatives and non-carbonate solvents as well have been widely investigated to
52
53 solve the sluggish ion transport in electrolyte bulk such as fluorinated carbonates,¹⁷⁻¹⁸ ethers,¹⁹
54
55 nitriles,²⁰⁻²² esters,²³⁻²⁷ or fluorinated esters.²⁸⁻²⁹ However, the improved LT performance has
56
57 been exclusively attributed to the high conductivity of the electrolyte bulk, and there has been
58
59
60

1
2
3
4 a lack of systematic study to pinpoint the limiting factors and electrolyte design principle for
5
6 low temperature applications.
7
8
9

10
11 In this report, a low-melting point butyronitrile (BN)-based electrolyte with enhanced
12 conductivity²⁷⁻²⁹ at low temperature has been systematically investigated. It reveals that instead
13 of improved conductivity, the limiting factor for LT mainly lies on the graphite anode.
14 Specifically, the SEI formation and its chemical composition are the dominating factors.
15 Lithium nitride (Li₃N)-containing SEI formed via the reduction of butyronitrile solvent³⁰⁻³² is
16 beneficial in decreasing the interfacial impedance of the anode. Lithium fluoride (LiF), known
17 as a stable component in SEI,³³⁻³⁴ acts as a resistor for ion conduction, and can be minimized
18 by controlling electrolyte formulations with nitrile solvent. This modified SEI layer enables
19 the cells to operate at -40°C, while conventional carbonate electrolyte could not operate at all.
20 This study provides in-depth insights on designing principal for high performance lithium-ion
21 batteries for low temperature application.
22
23
24
25
26
27
28
29
30
31
32
33
34
35
36
37
38
39
40
41
42
43
44
45
46
47
48
49
50
51
52
53
54
55
56
57
58
59
60

Results and Discussion

The graphite anode is more sensitive to LT performance than the $\text{LiNi}_{0.6}\text{Mn}_{0.2}\text{Co}_{0.2}\text{O}_2$ (NMC622) cathode as evidenced by the much lower (7%) capacity of the graphite/Li half cell at -20°C compared to 25°C , in contrast, the NMC622/Li half-cell showed a smaller capacity decrease (64%) as shown in **Figure 1a-1b**. During the normal operation of a lithium-ion battery, electrode reaction kinetics are retarded by various factors, and among them there are three main overpotentials: 1) activation overpotential (η_{act}), 2) concentration overpotential (η_{conc}), and 3) Ohmic resistance. Since ohmic resistance is largely dominated by the ionic conductivity of the electrolyte and not the electrodes, we only considered the activation overpotential and concentration overpotential, which directly affect the kinetics of electrochemical reactions in lithium-ion battery systems. **Figure 1c** shows the evolution of theoretical overpotential with current density. Activation overpotential can be expressed by the classical Butler-Volmer equation:³⁵

$$\eta_{act} = -\frac{RT}{(1-\alpha)nF}\ln J_0 + \frac{RT}{(1-\alpha)nF}\ln J, \quad (1)$$

where R is the ideal gas constant, α is transfer coefficient, n is number of electrons for the reaction, F is Faraday constant, J_0 is exchange current density, and J is applied current density. The exchange current density (J_0) means the degree of reversibility of an electrode reaction, it has an inverse relation to interfacial charge-transfer resistance. ($J_0 = \frac{RT}{nFR_{ct}}$, R_{ct} is an interfacial charge-transfer resistance of an electrode.)

Concentration overpotential can be derived from the law of diffusion and is given by the following equation:³⁶

$$\eta_{conc} = \frac{RT}{nF}\ln \frac{J_{lim} - J}{J_{lim}} \quad (2)$$

1
2
3
4 where J_{lim} is a limiting current density when surface ion concentration goes to zero. The
5
6 limiting current density (J_{lim}) has a proportional relation to the diffusion coefficient. ($J_{lim} =$
7
8 $\frac{nFD_{Li^+}c_{Li^+}}{\delta}$, where D_{Li^+} is a diffusion coefficient, c_{Li^+} is a concentration of Li ion in an
9
10 electrolyte, and δ is a distance between electrodes.) The top plot in **Figure 1c** shows evolution
11
12 of these two overpotentials and their sum when J_0 is 2 mAcm⁻² and J_{lim} is 10 mAcm⁻² at
13
14 room temperature. In this condition, the total overpotential stays low and slightly increases
15
16 governed by the activation overpotential at low-to-moderate current density, and as the current
17
18 density goes to J_{lim} , the total overpotential sharply increases governed by the concentration
19
20 overpotential. We assumed two different situations at low temperature. One is when J_{lim} drops
21
22 to 2 mAcm⁻². In this case, the total overpotential grows large even at low current density and
23
24 the cell would not exhibit any capacity as the potential directly hits the cut-off voltage. The
25
26 other is when J_0 drops to 2×10^{-3} mAcm⁻². The total overpotential becomes high at very low
27
28 current density and slightly increases until the current density goes to J_{lim} . From these
29
30 overpotential increase trends, we prioritized the electrolyte properties; 1) high ionic
31
32 conductivity and 2) low interfacial resistance.
33
34
35
36
37
38
39
40

41 To validate the above theory, we selected a nitrile-based electrolyte due to their high ionic
42
43 conductivities.²⁰⁻²¹ Butyronitrile (BN) containing electrolytes BN/FEC (1 M LiPF₆ in BN/FEC
44
45 (75/25 v/v)) and BN/EC+FEC (1 M LiPF₆ in BN/EC (75/25 v/v) + 5 wt% FEC) were studied
46
47 and compared with the conventional electrolyte Gen 2 which is 1.2 M LiPF₆ in EC/EMC (3/7
48
49 w/w). **Figure 2a** shows the ionic conductivities of these electrolytes at various temperatures.
50
51 While Gen 2 had the lowest ionic conductivity of 7.5×10^{-3} Scm⁻¹ at 20°C, BN/FEC and
52
53 BN/EC+FEC showed much higher ionic conductivity of 13×10^{-3} and 11.6×10^{-3} Scm⁻¹ at 20°C,
54
55 respectively, due to the high dielectric constant and the low viscosity of BN present in the
56
57 electrolytes. In addition, the activation energy (E_a) was calculated from the Arrhenius plots and
58
59
60

1
2
3
4 shown in **Figure 2b**. Compared to a high activation energy of 6.3 kJ mol^{-1} for Gen 2, BN/FEC
5 and BN/EC+FEC electrolytes showed lower activation energy of 4.5 kJmol^{-1} , indicating both
6
7 could maintain high ionic conductivity at lower temperatures. The high ionic conductivity and
8
9 low activation energy of BN-based electrolytes result in a low concentration overpotential at
10
11 low temperatures. We also conducted voltage holding test of NMC622/Graphite cells with
12
13 different electrolytes for electrochemical stability window. Although BN/FEC and
14
15 BN/EC+FEC showed a slightly higher leakage current than Gen 2, they have negligible values
16
17 up to 4.8 V (**Figure S1**).

18
19
20
21
22
23 Since interfacial resistance is largely determined by the SEI, we then analyzed the formation
24
25 of the SEI with various characterization methods in **Figure 3**. The reduction potential of Li^+ -
26
27 BN, Li^+ -EC, Li^+ -FEC were calculated to be 0.39, 0.58 and 0.80 V vs. Li/Li^+ , respectively
28
29 (**Figure 3a**). This trend in reduction potential is in good agreement with the reduction peak at
30
31 3.1 V, 3.0 V, and 2.65 V in the dQ/dV plots of NMC622/graphite cells during the 1st charging
32
33 cycle as shown in **Figure 3b**. It is worth noting that the BN solvent by itself could not form a
34
35 stable SEI layer, and a BN/EC (75/25 v/v) co-solvent electrolyte also showed a low initial
36
37 Coulombic efficiency (CE) due to the close reduction potential of EC and BN (**Figure S2**).
38
39 However, a robust SEI layer could be tuned by adding 5 wt% FEC as an additive to BN/EC.
40
41 Though FEC has a higher reduction potential than that of EC, the SEI is predominantly formed
42
43 by the reduction of the first Li^+ -coordinated solvation sheath, which according to MD
44
45 calculations, contains far more EC than FEC. Thus, the large contribution of EC to the SEI
46
47 layer formation is explained by MD results that show the Li^+ coordination number of EC (0.55)
48
49 is much higher than FEC (0.03) in BN/EC+FEC electrolyte system (**Figure 3c**). The
50
51 coordination numbers of electrolyte components at various temperatures in BN/FEC or
52
53 BN/EC+FEC electrolyte system are summarized in **Table S1-S2** in supporting information.
54
55
56
57
58
59
60

1
2
3
4 The effect of the electrolytes/additive on SEI chemical composition was examined by X-ray
5 photoelectron spectroscopy (XPS) after three formation cycles (**Figure 3d**). The peaks in C 1s
6 spectra at 289.6 eV, 288.4 eV, 286.8 eV, 285.8 eV, and 284.8 eV are assigned to OCOO, O–
7 C=O, C=O, C–O–C, and C–C, respectively, and are attributed to EC and FEC decomposition
8 products. No significant difference was observed between Gen 2, BN/FEC, and BN/EC+FEC
9 electrolyte, which share a high portion of carbonate-derived functional groups. In the case of F
10 1s and N 1s spectra, the F 1s peaks at 687.8 eV, 684.7 eV and N 1s peak at 399 eV are assigned
11 to $\text{Li}_x\text{PO}_y\text{F}_z$, LiF, and Li_3N , respectively. Compared to Gen 2, the SEI layer formed by BN/FEC
12 and BN/EC+FEC electrolyte is composed of new species Li_3N , which is a known SEI
13 component with high ionic conductivity.^{30, 32} In addition, BN/EC+FEC electrolyte cycled
14 graphite anode showed a lower concentration of LiF in SEI layer than that formed by BN/FEC
15 co-solvent electrolyte.

16
17
18
19
20
21
22
23
24
25
26
27
28
29
30
31
32
33 **Figure 4** shows the electrochemical impedance spectroscopy (EIS) for NMC622/graphite
34 measured at 50% state of charge (SOC) (or 3.7 V) after three formation cycles. It is evident
35 that as temperature decreases, the total cell resistance increases due to the lower thermal energy
36 available for electrochemical reaction. To separate each resistance contribution to the
37 performance, we deconvoluted the measured data with an equivalent circuit with constant
38 phase elements which are bulk electrolyte (R_{elect}), SEI layer (R_{SEI}), CEI layer (R_{CEI}), charge-
39 transfer at anode ($R_{\text{ct-anode}}$) and charge-transfer at cathode ($R_{\text{ct-cathode}}$). We matched the
40 frequencies of each resistance component by using anode and cathode symmetric cells (**Figure**
41 **S3** in supporting information). EIS data were well fitted with the equivalent circuit at -15°C
42 verifying the fitting model (**Figure S4**), and the fitting results of parameters are provided in
43 **Table S3-S5**.

1
2
3
4 BN/FEC and BN/EC+FEC electrolyte cells showed significantly smaller total resistance
5 compared to Gen 2 at all testing temperatures (**Figure 4a-4c**), indicating their lower interfacial
6 resistance and lower overpotential during operation. When it comes to each resistance
7 contribution (**Figure S4**), BN/EC+FEC had a much smaller $R_{\text{ct-anode}}$ than BN/FEC due to the
8 modified SEI layer with a lower concentration of LiF. We further analyzed the temperature
9 effect on each resistance component by the Arrhenius plots (**Figure 4d-4f**). The slope of $\log R$
10 vs $1000/T$ plot indicates the activation energy (E_a) for the reaction, meaning the temperature
11 dependence of the reaction. A higher E_a leads to a slower reaction and greater resistance at low
12 temperature. For Gen 2 electrolyte cell, the activation energies of R_{SEI} , R_{CEI} , $R_{\text{ct-anode}}$ and $R_{\text{ct-}}$
13 R_{cathode} are 0.8, 11.3, 24.4 and 25.3 kJmol^{-1} , respectively, indicating that charge-transfer
14 resistance becomes a main limiting factor at low temperatures. While BN/FEC has a similar
15 $R_{\text{ct-anode}}$ activation energy of 24.3 kJmol^{-1} as Gen 2, BN/EC+FEC has a lower activation energy
16 of 22.1 kJmol^{-1} . Considering that the overpotential on graphite anode is a limiting factor at low
17 temperature, the significantly lower $R_{\text{ct-anode}}$ activation energy of BN/EC+FEC enables superior
18 rate capabilities at low temperature, confirming the effectiveness of the modified SEI layer.
19
20
21
22
23
24
25
26
27
28
29
30
31
32
33
34
35
36
37
38
39

40 At room temperature, when various currents were applied from C/10 to C/3, C/2, 1C and 2C,
41 Gen 2 and BN/FEC and BN/EC+FEC cells showed similar performance. However, when the
42 temperature decreased to -20°C , with the same C-rate, Gen 2 showed significantly lower
43 capacity. In contrast, BN/EC+FEC electrolyte cell showed the best rate capability and delivered
44 129, 102, 89, 63, and 29 mAhg^{-1} at C/10 to C/3, C/2, 1C and 2C. Interestingly, when
45 temperature further decreased to -40°C , even C/5 current was applied, Gen 2 cell only showed
46 8 mAhg^{-1} cell capacity while the BN/EC+FEC cell still retained high capacity of 41 mAhg^{-1}
47 due to its lower interfacial resistance. To correlate the effect of a modified SEI layer with
48 overpotential, we calculated overpotential evolution's dependence on C-rate (**Figure 5d-5f**) at
49
50
51
52
53
54
55
56
57
58
59
60

1
2
3
4 50% of normalized capacity. While the electrolytes exhibited a similar overpotential increase
5
6 at room temperature, BN/EC+FEC showed a lower overpotential increase at -20 and -40°C
7
8 (**Figure S5**), reconfirming its lower interfacial resistance during low temperature operation.

9
10
11
12 **Figure 6a** summarizes the galvanostatic cycling results with C/3 at room temperature. While
13
14 Gen 2 showed stable cyclability retaining 98% of its initial capacity after 100 cycles, BN/FEC
15
16 and BN/EC+FEC exhibited a slight capacity fade and only retained 86% and 91% of their
17
18 original capacity after 100 cycles (**Figure S6**) due to the continuous BN solvent reduction
19
20 during cycling and low thermal stability which is also observed at high temperature of 40°C
21
22 (**Figure S7**). Lower CEs were also evident for both BN/FEC and BN/EC+FEC cells compared
23
24 to that of Gen 2 (**Figure S8**). However, at -40°C , BN/EC+FEC exhibited a remarkably high
25
26 capacity retention of 97% after 100 cycles, compared to only 61% for Gen 2 (**Figure 6a**).
27
28 Because a large overpotential at the anode causes Li plating and electrolyte decomposition,
29
30 which lowers CEs and capacity retention, the low interfacial resistance of BN/EC+FEC causes
31
32 it to outperform Gen 2 at low temperature. This was directly observed from the charged
33
34 graphite electrodes after 5 cycles at -40°C (**Figure S9**).

35
36
37
38
39
40
41 To elucidate the correlation of the SEI layer and low temperature performance, cycling test
42
43 with a preformed SEI by either Gen 2 or BN/EC+FEC were performed. After three formation
44
45 cycles at room temperature, the cells were reassembled with new electrolyte and cycled at $-$
46
47 40°C . The Gen 2 electrolyte cell (**Figure 6c**) with a SEI layer formed by Gen 2 showed a slight
48
49 degradation maintaining 87% of initial capacity during 30 cycles, while the same electrolyte
50
51 cell with SEI layer formed by BN/EC+FEC didn't show capacity decay. Similarly,
52
53 BN/EC+FEC electrolyte cell (**Figure 6d**) with SEI layer formed by Gen 2 and by BN/EC+FEC
54
55 showed same initial capacity of 66 mAhg^{-1} (which is much higher than 45 mAhg^{-1} for Gen 2
56
57 cell). At the end of 100 cycles, the cell with SEI layer formed by Gen 2 exhibited a dramatic
58
59
60

1
2
3
4 decay with only 77% of capacity retention even in 30 cycles, while the cell with SEI layer
5
6 formed by BN/EC+FEC displayed a high capacity retention of 98% with an average CE close
7
8 to 100%, confirming the significant role of SEI in the cell performance at low temperature.
9
10
11
12
13
14

15 **Conclusions**

16
17
18
19 In summary, the effect of the graphite SEI on the low temperature performance of lithium-ion
20
21 batteries has been systematically studied. The overpotential resulting from a resistive SEI and
22
23 high charge transfer resistance dictates the cell performance at low temperature. By formulating
24
25 a nitrile-based electrolyte 1.0 M LiPF₆ in BN/EC+FEC, we demonstrate that the new SEI
26
27 composed of Li₃N and LiF significantly lowers the anode charge-transfer resistance with a low
28
29 activation energy, resulting in superior rate capability and cyclability even at -40°C. This
30
31 investigation provides a deep insight in designing principal of new electrolytes for low
32
33 temperature
34
35 Li-ion
36
37
38
39
40
41
42
43
44
45
46
47
48
49
50
51
52
53
54
55
56
57
58
59
60
batteries.

Experimental Section

Materials: Butyronitrile (BN), ethylene carbonate (EC) and fluoroethylene carbonate (FEC) were purchased from Sigma Aldrich. All solvents used in this study were purified by vacuum distillation and then dried by adding 4 Å molecular sieves before use. Gen 2 electrolyte is 1.2 M LiPF₆ in EC/EMC (3/7 w/w ratio). All electrodes were provided by Argonne's Cell Analysis, Modeling and Prototyping (CAMP) facility. The cathode (NMC622) was composed of 90 wt% Li(Ni_{0.6}Mn_{0.2}Co_{0.2})O₂, 5 wt% polyvinylidene fluoride binder (PVdF, Solvay) and 5 wt% C45 conductive carbon casted on an aluminum foil with a mass loading of 9.78 mg/cm². The graphite anode was composed of 91.83 wt% Superior graphite (SLC1520P), 6 wt% PVdF binder (Kureha, 9300), 0.17 wt% oxalic acid additive, and 2 wt% C45 conductive carbon casted on a copper foil with a mass loading of 6.38 mg/cm². All electrodes were dried at 110°C under vacuum for overnight. Celgard 2500 was used as the separator. The diameters of the cathode, anode and separator were 14, 15, and 16 mm, respectively.

Electrochemical Measurements: The electrochemical performance was evaluated by 2032 coin cells. The full cells were composed of NMC622 cathode and graphite anode with different electrolytes. The cell assembly was conducted in an argon-filled glovebox. All the galvanostatic cycling was performed at 2.7 ~ 4.2 V following three initial C/10 formation cycles using Neware battery tester. The electrochemical impedance spectroscopy (EIS) was obtained and fitted using a Solartron analyzer operated between 0.01 Hz and 1 MHz with amplitude of 10 mV.

Characterization: The cycled cells were disassembled in an argon-filled glovebox. The graphite electrodes were obtained after three formation cycles with Gen 2, BN/FEC or BN/EC+FEC electrolytes. The electrodes were rinsed with dimethyl carbonate for Gen 2 cycled electrodes or BN for BN/FEC and BN/EC+FEC cycled electrodes, and characterized after

1
2
3
4 vacuum dried. X-ray photoelectron spectroscopy (XPS) was conducted in the fixed analyzer
5
6 transmission mode using an Al K α radiation ($h\nu = 1486.6$ eV, 100 μm beam, 25W) with Ar⁺
7
8 and electron beam sample neutralization. XPS spectra were calibrated to the C-C bond at 284.7
9
10 eV.
11
12

13
14 *DFT calculation:* DFT calculation: Structure optimizations of LiEC, LiFEC, and LiBN were
15
16 performed with the ω B97X-d functional and def2-TZVPPD basis set in the QChem software
17
18 package.³⁷ DFT calculations were performed with the SMD implicit solvent model
19
20 parameterized to BN. Structures for LiEC and LiFEC were taken from the LIBE dataset.³⁸ For
21
22 BN, the bare solvent was first optimized at -1 charge before Li was inserted.
23
24

25
26 *MD simulation:* We acquired OPLS force field parameters for BN from LigParGen³⁹ and
27
28 calculated partial charges with a Restrained Electrostatic Potential (RESP) fit using
29
30 Antechamber.⁴⁰ The RESP calculation used a geometry optimized structure calculated with
31
32 Gaussian 16 at the B3LYP/aug-cc-pvdz level of theory. BN partial charges were scaled to 80%
33
34 of their initial value so that the simulated density of BN matched the experimental density.
35
36 OPLS force field parameters for EC, FEC, and LiPF₆ were taken from Hou et al.⁴¹ We
37
38 performed molecular dynamics calculations with the Large Scale Atomic/Molecular Massively
39
40 Parallel Simulator (LAMMPS) package.⁴² A random initial configuration of the molecular
41
42 system was generated with PACKMOL⁴³ followed by an energy minimization with conjugate
43
44 gradient descent. Each simulation began with a 1 ns pressure equilibration in the NPT ensemble
45
46 at 1 atm, 298 K. The system was then annealed by raising the temperature to 400 K, holding at
47
48 400 K, and then returning 298 K, each for 1 ns. After this equilibration, the production part of
49
50 the simulation ran for 5 ns. All solvation structure geometries and statistics were taken from
51
52 the production run.
53
54
55
56
57

58 **Supporting Information**

59
60

1
2
3
4 Voltage holding test, voltage profiles, coordination numbers, Bode plots, Nyquist plots, EIS
5
6 fitting results, normalized voltage profiles, cycling performance at a high temperature,
7
8 Coulombic efficiency, photographs of cycled electrodes.
9

10 11 **Acknowledgement** 12

13 Support from Peter Faguy and Mallory Clites at Vehicle Technologies Office (VTO), Office
14
15 of Energy Efficiency and Renewable Energy, U.S. Department of Energy is gratefully
16
17 acknowledged. NMC532 electrodes were fabricated at Argonne's Cell Analysis, Modeling,
18
19 and Prototyping (CAMP) Facility, which is fully supported by VTO within the core funding of
20
21 the Applied Battery Research (ABR) for Transportation Program. The submitted manuscript
22
23 has been created by UChicago Argonne, LLC, Operator of Argonne National Laboratory,
24
25 which is supported by the Office of Science, U.S. Department of Energy under Contract No.
26
27 DE-AC02-06CH11357.
28
29
30
31
32
33
34
35
36
37
38
39
40
41
42
43
44
45
46
47
48
49
50
51
52
53
54
55
56
57
58
59
60

Reference

1. Choi, J. W.; Aurbach, D., Promise and Reality of Post-Lithium-Ion Batteries with High Energy Densities. *Nature Reviews Materials* **2016**, *1* (4), 16013.
2. Etacheri, V.; Marom, R.; Elazari, R.; Salitra, G.; Aurbach, D., Challenges in the Development of Advanced Li-Ion Batteries: a Review. *Energy & Environmental Science* **2011**, *4* (9), 3243-3262.
3. Dunn, B.; Kamath, H.; Tarascon, J.-M., Electrical Energy Storage for the Grid: A Battery of Choices. *Science* **2011**, *334* (6058), 928-935.
4. Bandhauer, T. M.; Garimella, S.; Fuller, T. F., A Critical Review of Thermal Issues in Lithium-Ion Batteries. *Journal of The Electrochemical Society* **2011**, *158* (3), R1.
5. Gupta, A.; Manthiram, A., Designing Advanced Lithium-Based Batteries for Low-Temperature Conditions. *Advanced energy materials* **2020**, *10* (38), 2001972.
6. Jow, T. R.; Delp, S. A.; Allen, J. L.; Jones, J.-P.; Smart, M. C., Factors Limiting Li⁺ Charge Transfer Kinetics in Li-Ion Batteries. *Journal of The Electrochemical Society* **2018**, *165* (2), A361-A367.
7. Rodrigues, M.-T. F.; Babu, G.; Gullapalli, H.; Kalaga, K.; Sayed, F. N.; Kato, K.; Joyner, J.; Ajayan, P. M., A Materials Perspective on Li-Ion Batteries at Extreme Temperatures. *Nature Energy* **2017**, *2* (8), 17108.
8. Ren, D.; Smith, K.; Guo, D.; Han, X.; Feng, X.; Lu, L.; Ouyang, M.; Li, J., Investigation of Lithium Plating-Stripping Process in Li-Ion Batteries at Low Temperature Using an Electrochemical Model. *Journal of The Electrochemical Society* **2018**, *165* (10), A2167-A2178.
9. Zhang, S. S.; Xu, K.; Jow, T. R., Electrochemical Impedance Study on the Low Temperature of Li-Ion Batteries. *Electrochimica Acta* **2004**, *49* (7), 1057-1061.
10. Li, Q.; Cao, Z.; Wahyudi, W.; Liu, G.; Park, G.-T.; Cavallo, L.; Anthopoulos, T. D.; Wang, L.; Sun, Y.-K.; Alshareef, H. N.; Ming, J., Unraveling the New Role of an Ethylene Carbonate Solvation Shell in Rechargeable Metal Ion Batteries. *ACS Energy Letters* **2021**, *6* (1), 69-78.
11. Shen, C.; Wang, S.; Jin, Y.; Han, W.-Q., In Situ AFM Imaging of Solid Electrolyte Interfaces on HOPG with Ethylene Carbonate and Fluoroethylene Carbonate-Based Electrolytes. *ACS Applied Materials & Interfaces* **2015**, *7* (45), 25441-25447.
12. Smart, M. C.; Whitacre, J. F.; Ratnakumar, B. V.; Amine, K., Electrochemical Performance and Kinetics of Li_{1+x}(Co_{1/3}Ni_{1/3}Mn_{1/3})_{1-x}O₂ Cathodes and Graphite Anodes in Low-Temperature Electrolytes. *Journal of Power Sources* **2007**, *168* (2), 501-508.
13. Li, Q.; Jiao, S.; Luo, L.; Ding, M. S.; Zheng, J.; Cartmell, S. S.; Wang, C.-M.; Xu, K.; Zhang, J.-G.; Xu, W., Wide-Temperature Electrolytes for Lithium-Ion Batteries. *ACS Applied Materials & Interfaces* **2017**, *9* (22), 18826-18835.
14. Plichta, E. J.; Behl, W. K., A Low-Temperature Electrolyte for Lithium and Lithium-Ion Batteries. *Journal of Power Sources* **2000**, *88* (2), 192-196.
15. Huang, C. K.; Sakamoto, J. S.; Wolfenstine, J.; Surampudi, S., The Limits of Low-Temperature Performance of Li-Ion Cells. *Journal of The Electrochemical Society* **2000**, *147* (8), 2893.
16. Smart, M. C.; Ratnakumar, B. V.; Whitcanack, L. D.; Chin, K. B.; Surampudi, S.; Croft, H.; Tice, D.; Staniewicz, R., Improved Low-Temperature Performance of Lithium-Ion Cells with Quaternary Carbonate-Based Electrolytes. *Journal of Power Sources* **2003**, *119-121*, 349-358.
17. Liao, L.; Cheng, X.; Ma, Y.; Zuo, P.; Fang, W.; Yin, G.; Gao, Y., Fluoroethylene

Carbonate as Electrolyte Additive to Improve Low Temperature Performance of LiFePO₄ Electrode. *Electrochimica Acta* **2013**, *87*, 466-472.

18. Wang, Z.; Sun, Z.; Shi, Y.; Qi, F.; Gao, X.; Yang, H.; Cheng, H.-M.; Li, F., Ion-Dipole Chemistry Drives Rapid Evolution of Li Ions Solvation Sheath in Low-Temperature Li Batteries. *Advanced Energy Materials* **2021**, *11* (28), 2100935.

19. Fan, X.; Ji, X.; Chen, L.; Chen, J.; Deng, T.; Han, F.; Yue, J.; Piao, N.; Wang, R.; Zhou, X.; Xiao, X.; Chen, L.; Wang, C., All-Temperature Batteries Enabled by Fluorinated Electrolytes with Non-Polar Solvents. *Nature Energy* **2019**, *4* (10), 882-890.

20. Cho, Y.-G.; Kim, Y.-S.; Sung, D.-G.; Seo, M.-S.; Song, H.-K., Nitrile-Assistant Eutectic Electrolytes for Cryogenic Operation of Lithium Ion Batteries at Fast Charges and Discharges. *Energy & Environmental Science* **2014**, *7* (5), 1737-1743.

21. Hilbig, P.; Ibing, L.; Winter, M.; Cekic-Laskovic, I., Butyronitrile-Based Electrolytes for Fast Charging of Lithium-Ion Batteries. *Energies* **2019**, *12* (15), 2869.

22. Hu, P.; Chai, J.; Duan, Y.; Liu, Z.; Cui, G.; Chen, L., Progress in Nitrile-Based Polymer Electrolytes for High Performance Lithium Batteries. *Journal of Materials Chemistry A* **2016**, *4* (26), 10070-10083.

23. Cai, G.; Holoubek, J.; Xia, D.; Li, M.; Yin, Y.; Xing, X.; Liu, P.; Chen, Z., An Ester Electrolyte for Lithium-Sulfur Batteries Capable of Ultra-Low Temperature Cycling. *Chemical Communications* **2020**, *56* (64), 9114-9117.

24. Cho, Y.-G.; Li, M.; Holoubek, J.; Li, W.; Yin, Y.; Meng, Y. S.; Chen, Z., Enabling the Low-Temperature Cycling of NMC||Graphite Pouch Cells with an Ester-Based Electrolyte. *ACS Energy Letters* **2021**, *6* (5), 2016-2023.

25. Dong, X.; Guo, Z.; Guo, Z.; Wang, Y.; Xia, Y., Organic Batteries Operated at -70°C. *Joule* **2018**, *2* (5), 902-913.

26. Smart, M. C.; Ratnakumar, B. V.; Chin, K. B.; Whitcanack, L. D., Lithium-Ion Electrolytes Containing Ester Cosolvents for Improved Low Temperature Performance. *Journal of The Electrochemical Society* **2010**, *157* (12), A1361.

27. Smart, M. C.; Ratnakumar, B. V.; Surampudi, S., Use of Organic Esters as Cosolvents in Electrolytes for Lithium-Ion Batteries with Improved Low Temperature Performance. *Journal of The Electrochemical Society* **2002**, *149* (4), A361.

28. Holoubek, J.; Yu, M.; Yu, S.; Li, M.; Wu, Z.; Xia, D.; Bhaladhare, P.; Gonzalez, M. S.; Pascal, T. A.; Liu, P.; Chen, Z., An All-Fluorinated Ester Electrolyte for Stable High-Voltage Li Metal Batteries Capable of Ultra-Low-Temperature Operation. *ACS Energy Letters* **2020**, *5* (5), 1438-1447.

29. Yang, Y.; Li, P.; Wang, N.; Fang, Z.; Wang, C.; Dong, X.; Xia, Y., Fluorinated Carboxylate Ester-Based Electrolyte for Lithium Ion Batteries Operated at Low Temperature. *Chemical Communications* **2020**, *56* (67), 9640-9643.

30. Boukamp, B. A.; Huggins, R. A., Lithium Ion Conductivity in Lithium Nitride. *Physics Letters A* **1976**, *58* (4), 231-233.

31. Chen, K.; Pathak, R.; Gurung, A.; Adhamash, E. A.; Bahrami, B.; He, Q.; Qiao, H.; Smirnova, A. L.; Wu, J. J.; Qiao, Q.; Zhou, Y., Flower-Shaped Lithium Nitride as a Protective Layer via Facile Plasma Activation for Stable Lithium Metal Anodes. *Energy Storage Materials* **2019**, *18*, 389-396.

32. Tapia-Ruiz, N.; Gordon, A. G.; Jewell, C. M.; Edwards, H. K.; Dunnill, C. W.; Blackman, J. M.; Snape, C. P.; Brown, P. D.; MacLaren, I.; Baldoni, M.; Besley, E.; Titman, J. J.; Gregory, D. H., Low Dimensional Nanostructures of Fast Ion Conducting Lithium Nitride. *Nature Communications* **2020**, *11* (1), 4492.

33. He, M.; Guo, R.; Hobold, G. M.; Gao, H.; Gallant, B. M., The Intrinsic Behavior of Lithium Fluoride in Solid Electrolyte Interphases on Lithium. *Proceedings of the National*

1
2
3
4
5
6
7
8
9
10
11
12
13
14
15
16
17
18
19
20
21
22
23
24
25
26
27
28
29
30
31
32
33
34
35
36
37
38
39
40
41
42
43
44
45
46
47
48
49
50
51
52
53
54
55
56
57
58
59
60

Academy of Sciences **2020**, *117* (1), 73.

34. Yoo, D.-J.; Yang, S.; Kim, K. J.; Choi, J. W., Fluorinated Aromatic Diluent for High-Performance Lithium Metal Batteries. *Angewandte Chemie International Edition* **2020**, *59* (35), 14869-14876.

35. Dickinson, E. J. F.; Wain, A. J., The Butler-Volmer Equation in Electrochemical Theory: Origins, Value, and Practical Application. *Journal of Electroanalytical Chemistry* **2020**, *872*, 114145.

36. Vogt, H., The Concentration Overpotential of Gas Evolving Electrodes as a Multiple Problem of Mass Transfer. *Journal of The Electrochemical Society* **1990**, *137* (4), 1179-1184.

37. Shao, Y.; Gan, Z.; Epifanovsky, E.; Gilbert, A. T. B.; Wormit, M.; Kussmann, J.; Lange, A. W.; Behn, A.; Deng, J.; Feng, X.; Ghosh, D.; Goldey, M.; Horn, P. R.; Jacobson, L. D.; Kaliman, I.; Khaliullin, R. Z.; Kuš, T.; Landau, A.; Liu, J.; Proynov, E. I.; Rhee, Y. M.; Richard, R. M.; Rohrdanz, M. A.; Steele, R. P.; Sundstrom, E. J.; Woodcock, H. L.; Zimmerman, P. M.; Zuev, D.; Albrecht, B.; Alguire, E.; Austin, B.; Beran, G. J. O.; Bernard, Y. A.; Berquist, E.; Brandhorst, K.; Bravaya, K. B.; Brown, S. T.; Casanova, D.; Chang, C.-M.; Chen, Y.; Chien, S. H.; Closser, K. D.; Crittenden, D. L.; Diedenhofen, M.; DiStasio, R. A.; Do, H.; Dutoi, A. D.; Edgar, R. G.; Fatehi, S.; Fusti-Molnar, L.; Ghysels, A.; Golubeva-Zadorozhnaya, A.; Gomes, J.; Hanson-Heine, M. W. D.; Harbach, P. H. P.; Hauser, A. W.; Hohenstein, E. G.; Holden, Z. C.; Jagau, T.-C.; Ji, H.; Kaduk, B.; Khistyayev, K.; Kim, J.; Kim, J.; King, R. A.; Klunzinger, P.; Kosenkov, D.; Kowalczyk, T.; Krauter, C. M.; Lao, K. U.; Laurent, A. D.; Lawler, K. V.; Levchenko, S. V.; Lin, C. Y.; Liu, F.; Livshits, E.; Lochan, R. C.; Luenser, A.; Manohar, P.; Manzer, S. F.; Mao, S.-P.; Mardirossian, N.; Marenich, A. V.; Maurer, S. A.; Mayhall, N. J.; Neuscammann, E.; Oana, C. M.; Olivares-Amaya, R.; O'Neill, D. P.; Parkhill, J. A.; Perrine, T. M.; Peverati, R.; Prociuk, A.; Rehn, D. R.; Rosta, E.; Russ, N. J.; Sharada, S. M.; Sharma, S.; Small, D. W.; Sodt, A.; Stein, T.; Stück, D.; Su, Y.-C.; Thom, A. J. W.; Tsuchimochi, T.; Vanovschi, V.; Vogt, L.; Vydrov, O.; Wang, T.; Watson, M. A.; Wenzel, J.; White, A.; Williams, C. F.; Yang, J.; Yeganeh, S.; Yost, S. R.; You, Z.-Q.; Zhang, I. Y.; Zhang, X.; Zhao, Y.; Brooks, B. R.; Chan, G. K. L.; Chipman, D. M.; Cramer, C. J.; Goddard, W. A.; Gordon, M. S.; Hehre, W. J.; Klamt, A.; Schaefer, H. F.; Schmidt, M. W.; Sherrill, C. D.; Truhlar, D. G.; Warshel, A.; Xu, X.; Aspuru-Guzik, A.; Baer, R.; Bell, A. T.; Besley, N. A.; Chai, J.-D.; Dreuw, A.; Dunietz, B. D.; Furlani, T. R.; Gwaltney, S. R.; Hsu, C.-P.; Jung, Y.; Kong, J.; Lambrecht, D. S.; Liang, W.; Ochsenfeld, C.; Rassolov, V. A.; Slipchenko, L. V.; Subotnik, J. E.; Van Voorhis, T.; Herbert, J. M.; Krylov, A. I.; Gill, P. M. W.; Head-Gordon, M., Advances in Molecular Quantum Chemistry Contained in the Q-Chem 4 Program Package. *Molecular Physics* **2015**, *113* (2), 184-215.

38. Spotte-Smith, E. W. C.; Blau, S. M.; Xie, X.; Patel, H. D.; Wen, M.; Wood, B.; Dwaraknath, S.; Persson, K. A., Quantum Chemical Calculations of Lithium-Ion Battery Electrolyte and Interphase Species. *Scientific Data* **2021**, *8* (1), 203.

39. Dodda, L. S.; Cabeza de Vaca, I.; Tirado-Rives, J.; Jorgensen, W. L., LigParGen web server: An Automatic OPLS-AA Parameter Generator for Organic Ligands. *Nucleic Acids Research* **2017**, *45* (W1), W331-W336.

40. Wang, J.; Wang, W.; Kollman, P. A.; Case, D. A., Automatic Atom Type and Bond Type Perception in Molecular Mechanical Calculations. *Journal of Molecular Graphics and Modelling* **2006**, *25* (2), 247-260.

41. Hou, T.; Fong, K. D.; Wang, J.; Persson, K. A., The Solvation Structure, Transport Properties and Reduction Behavior of Carbonate-Based Electrolytes of Lithium-Ion Batteries. *Chemical Science* **2021**, *12* (44), 14740-14751.

42. Thompson, A. P.; Aktulga, H. M.; Berger, R.; Bolintineanu, D. S.; Brown, W. M.; Crozier, P. S.; in 't Veld, P. J.; Kohlmeyer, A.; Moore, S. G.; Nguyen, T. D.; Shan, R.; Stevens,

1
2
3
4 M. J.; Tranchida, J.; Trott, C.; Plimpton, S. J., LAMMPS - A Flexible Simulation Tool for
5 Particle-Based Materials Modeling at the Atomic, Meso, and Continuum scales. *Computer*
6 *Physics Communications* **2022**, *271*, 108171.

7
8 43. Martínez, L.; Andrade, R.; Birgin, E. G.; Martínez, J. M., PACKMOL: A Package for
9 Building Initial Configurations for Molecular Dynamics Simulations. *Journal of*
10 *Computational Chemistry* **2009**, *30* (13), 2157-2164.
11
12
13
14
15
16
17
18
19
20
21
22
23
24
25
26
27
28
29
30
31
32
33
34
35
36
37
38
39
40
41
42
43
44
45
46
47
48
49
50
51
52
53
54
55
56
57
58
59
60

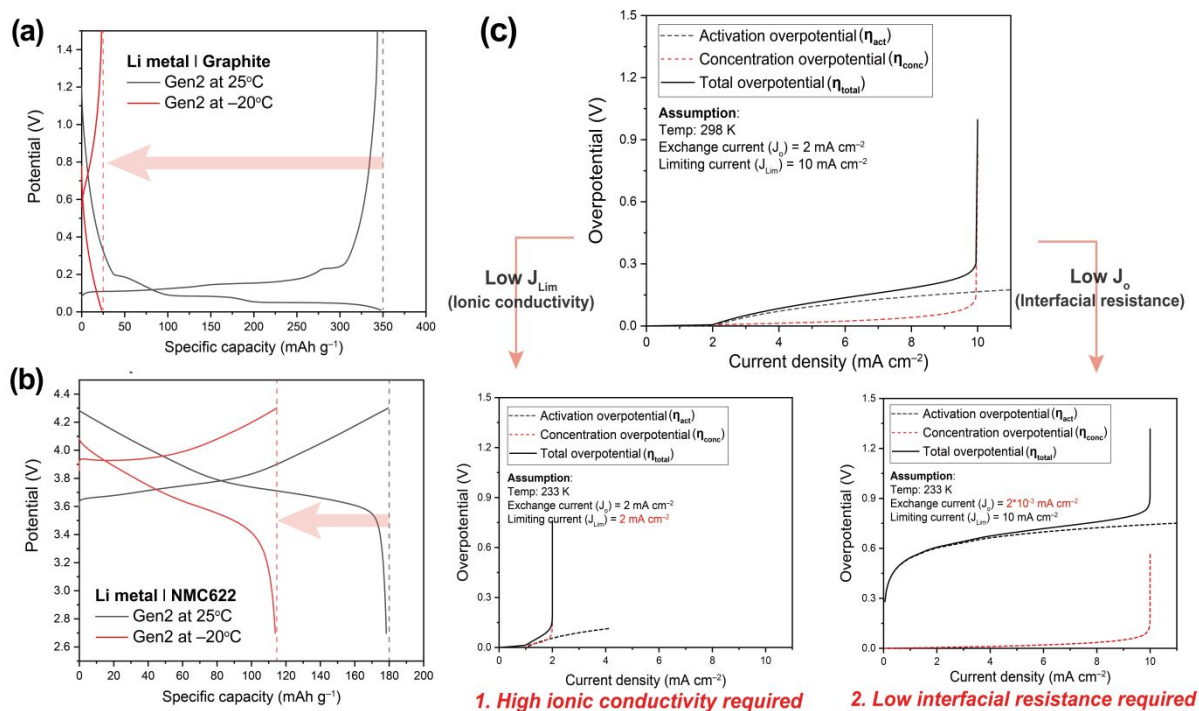


Figure 1. (a) Voltage profiles of graphite/Li half cells and (b) NMC622/Li half cells with Gen 2 electrolyte at 25°C and -20°C. (c) Theoretical lithium-ion battery overpotential evolution with limiting factors of electrolyte ionic conductivity and interfacial resistance at low temperature.

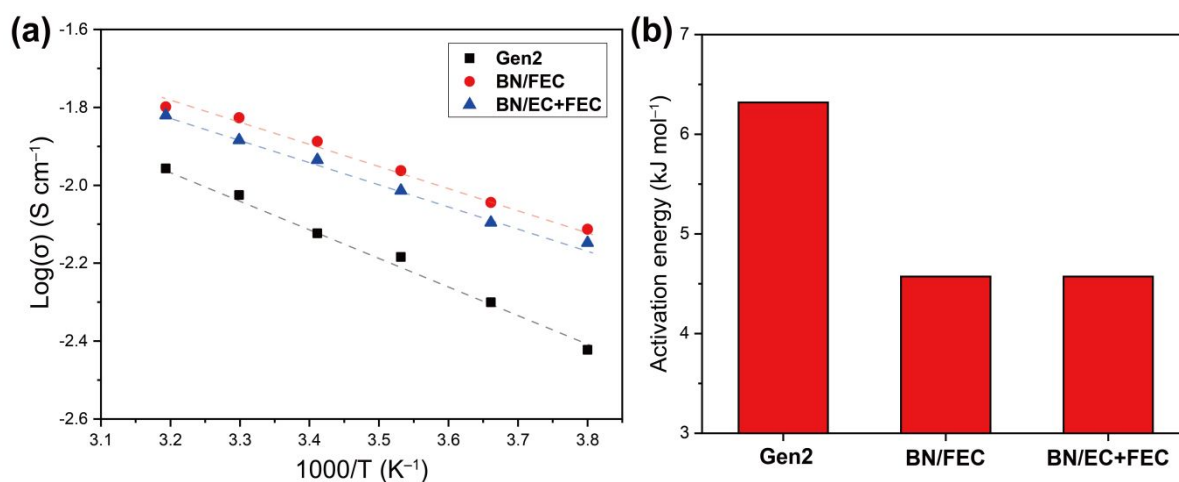


Figure 2. (a) Temperature dependence of ionic conductivity of Gen 2, 1M LiPF_6 BN/FEC (75/25 v/v), and 1M LiPF_6 BN/EC (75/25 v/v) + 5 wt% FEC electrolytes and (b) calculated activation energy (E_a) from plots in (a).

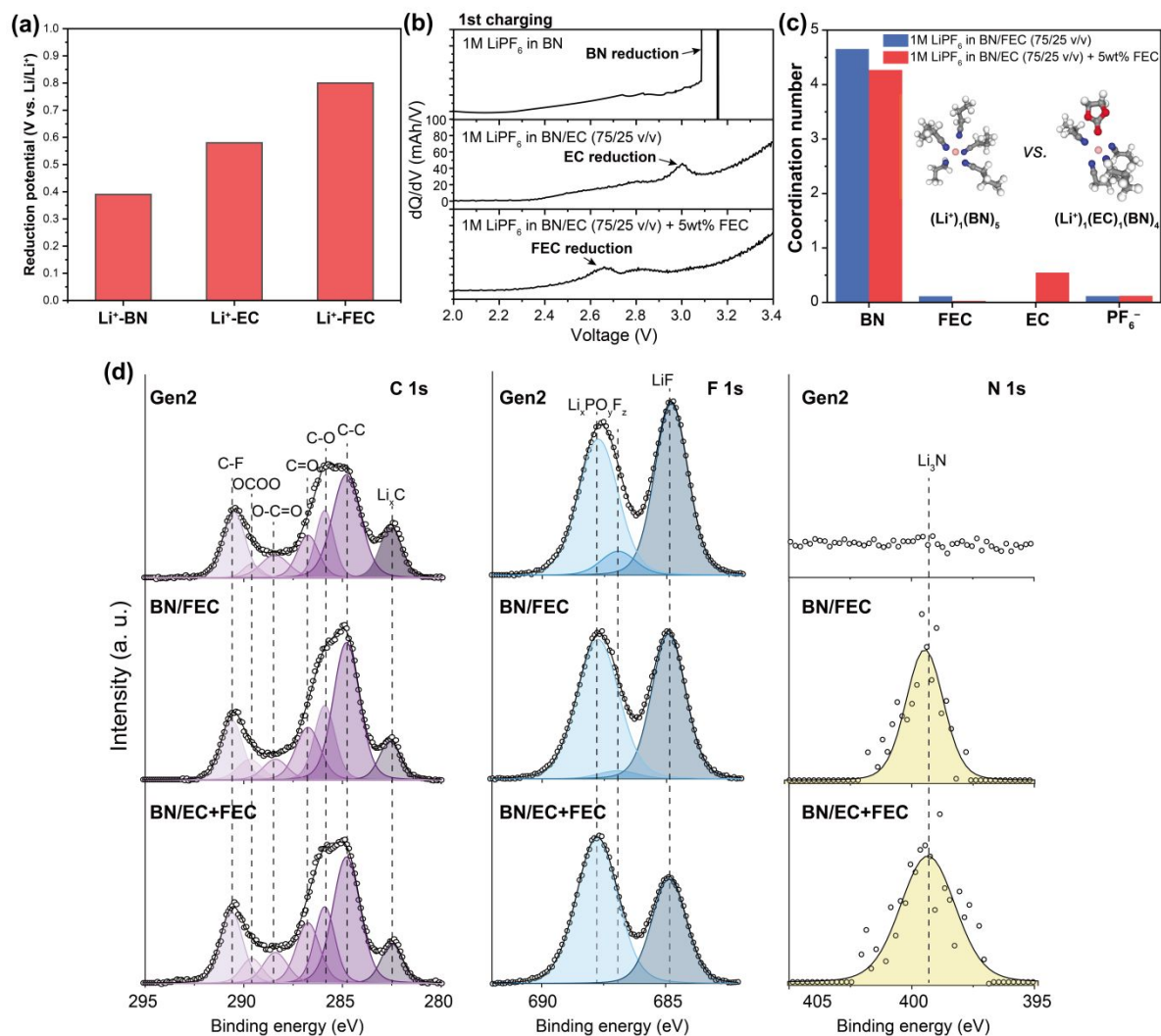


Figure 3. (a) Reduction potentials of Li^+ -BN, Li^+ -EC, and Li^+ -FEC, (b) dQ/dV profiles of the 1st charging cycle with Gen 2, 1M LiPF_6 BN/FEC (75/25 v/v), and 1M LiPF_6 BN/EC (75/25 v/v) + 5 wt% FEC electrolytes, (c) DFT calculated coordination number of electrolytes at 25°C, and (d) XPS spectra of C 1s, F 1s, and N 1s of cycled graphite anodes after three C/10 formation cycles with three electrolytes.

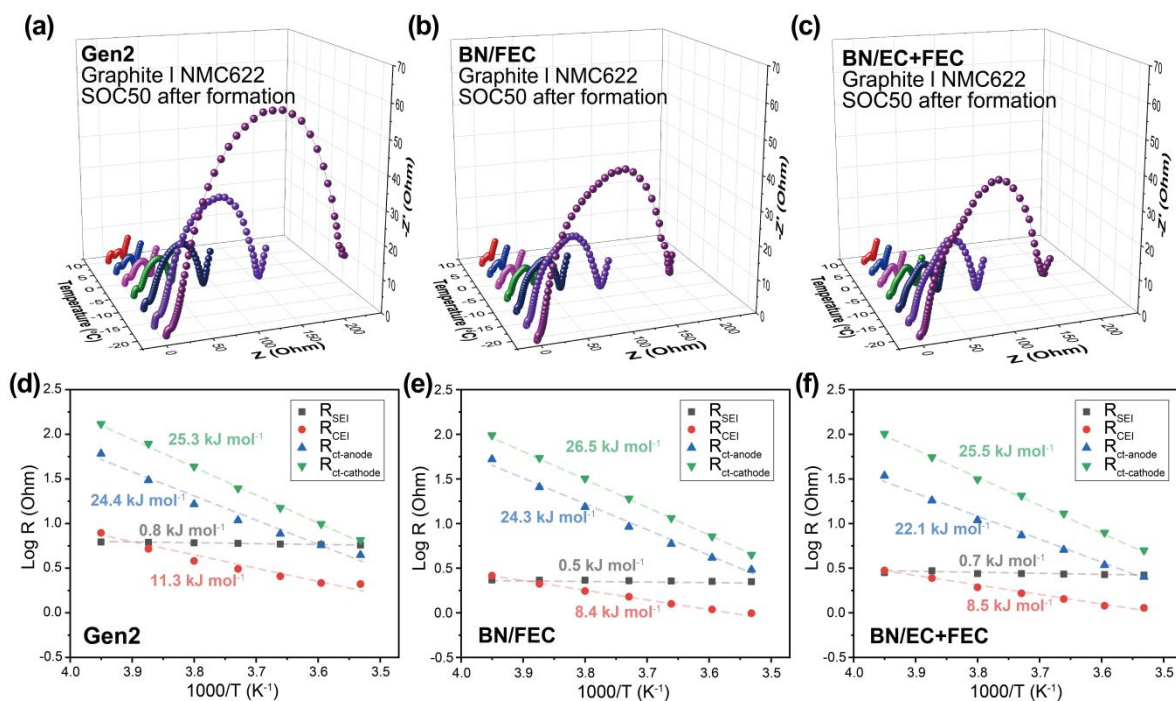


Figure 4. Nyquist plots of NMC622/graphite cells with (a) Gen 2, (b) BN/FEC, and (c) BN/EC+FEC electrolyte at various temperatures. Arrhenius plots of R_{SEI} , R_{CEI} , $R_{\text{ct-anode}}$, $R_{\text{ct-cathode}}$ for cells with (d) Gen 2, (e) BN/FEC, and (f) BN/EC+FEC electrolyte.

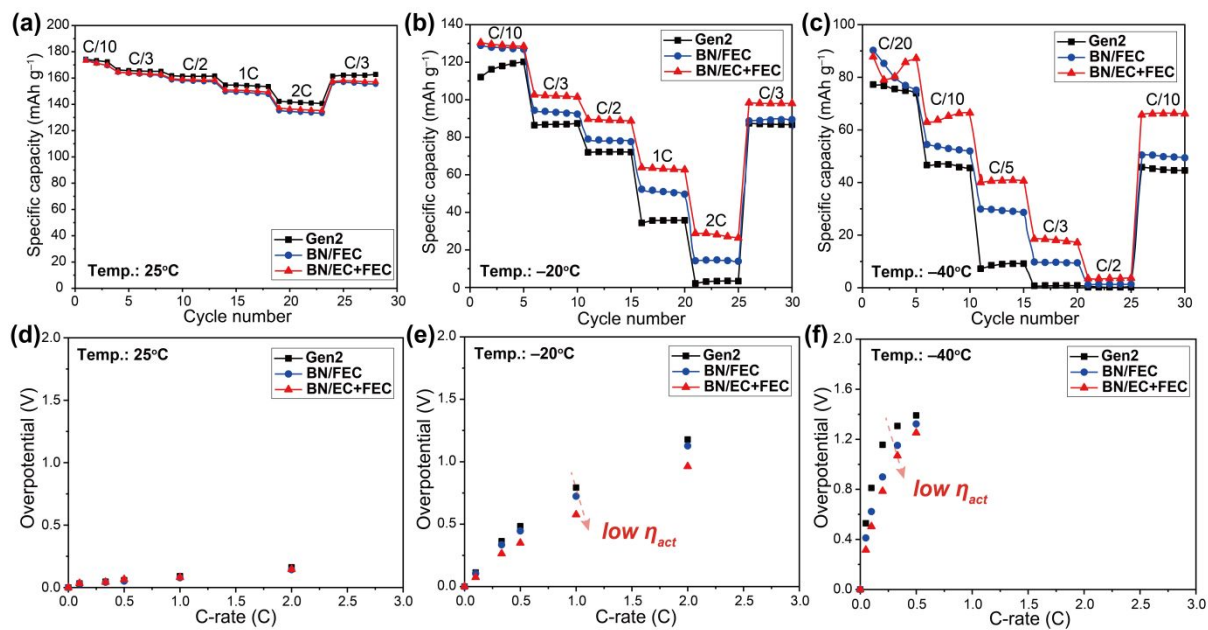


Figure 5. (a-c) C-rate capability for NMC622/graphite cells with different electrolytes, and (d-f) overpotential evolution with C-rate at 25°C, -20°C and -40°C.

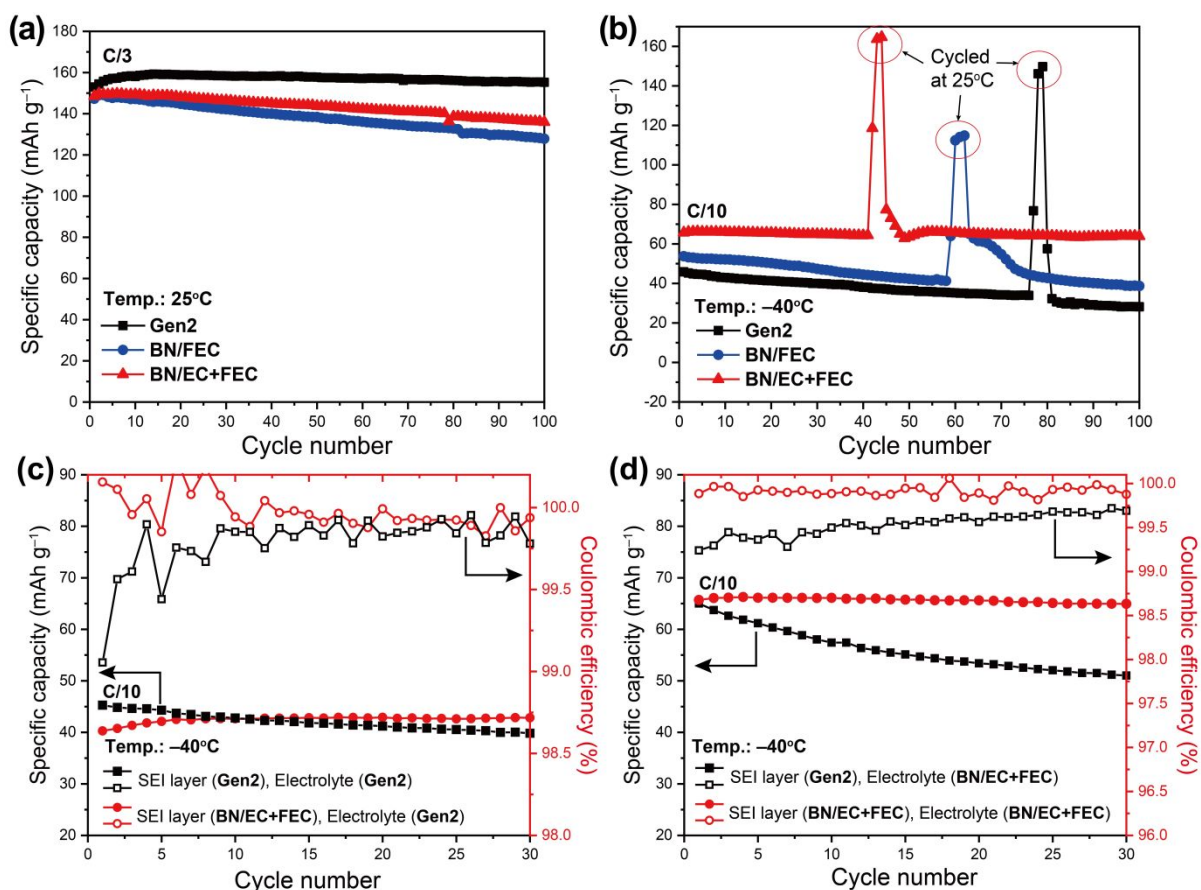


Figure 6. NMC622/graphite cell performance at (a) 25°C and (b) -40°C with different electrolytes, (c) -40°C cyclability and Coulombic efficiency of Gen 2 electrolyte cell with Gen 2 and BN/EC+FEC preformed SEI and (d) BN/EC+FEC electrolyte cell with Gen 2 and BN/EC+FEC preformed SEI.

Table of Contents (TOC)

